

The X–ray Spectrum of the Dwarf Nova SS Cyg in quiescence and outburst

C. Done¹ and J. P. Osborne²

¹*Department of Physics, University of Durham, South Road, Durham, DH1 3LE*

²*Department of Physics & Astronomy, University of Leicester, University Road, Leicester. LE1 7RH.*

2 August 2021

ABSTRACT

We reanalyse archival GINGA and ASCA X–ray data from SS Cyg in both quiescence and outburst, using multi–temperature plasma models for the continuum and line emission, together with their reflection from the X–ray illuminated white dwarf and accretion disk. Reflection is clearly detected in all the spectra, but its contribution is larger in the softer X–ray spectra seen in outburst than in quiescence. This supports models in which the quiescent inner disk is not present or not optically thick, so that the only reflector is the white dwarf surface rather than the white dwarf plus the disk. The amount of reflection in outburst is also more consistent with the hard X–rays forming a corona over the white dwarf surface rather than just an equatorial band. We detect partially ionized absorption in the ASCA outburst spectrum, which is probably the X–ray signature of the outflowing wind. The ASCA data also allow a detailed measure of the elemental abundances. We find that all detectable lines from the hot plasma (except perhaps Si and S) are a factor $\sim 2.5\times$ weaker than expected from solar abundances. We examine possible deviations from coronal equilibrium, but conclude that the heavy elements are truly underabundant in SS Cyg.

In quiescence the underlying intrinsic spectrum is consistent with a single temperature plasma. This conflicts with the expected cooling of the material, and requires that either the plasma is reheated or that the cooler emission is masked by absorption in an optically thin inner disk which affects only that part of the boundary layer emission below the disk. Such absorption is also required if the data are to match the theoretical models (Narayan & Popham 1993) for the quiescent hard X–ray emission. By contrast, the outburst spectrum is much softer and is dominated by the cooling components, so that it cannot be fit by a single temperature model. There are no readily available (or believable) theoretical models for the hard X–ray emission in outburst, but the emission observed can be described by material with a continuous temperature distribution. Although the outburst spectrum is much softer than the quiescent spectrum, the total luminosity of the X–ray component in both cases is similar, showing that the optically thin plasma emission is important even in outburst.

Key words: stars: individual: SS Cyg – cataclysmic variables – binaries: close – X-rays: accretion – X-rays: accretion

1 INTRODUCTION

The non–magnetic Cataclysmic Variable stars are systems where a white dwarf accretes via a disk from a Roche lobe filling, low mass, companion star. Dwarf novae (DN) are a subclass of these systems which show optical/UV outbursts of 2–6 magnitudes which are thought to be triggered by a disk instability giving a transient increase in the accretion rate (see e.g. the reviews by Cordova 1995, Warner 1995 and Osaki 1996). As the accreting material falls inwards,

the transition from the the disk velocity field to that of the white dwarf will lead to up to half of the accretion energy being dissipated (Pringle 1977, Kluzniak 1987).

Detailed theoretical models of the boundary layer emission are not well developed due to the inherent complexity of modelling the strongly shearing, probably turbulent transition region between the disk and white dwarf surface. However, general characteristics of the emission can be derived. Material leaves the inner edge of the disk with a temperature $\sim 10^5$ K, and then is heated (presumably by shocks)

as it joins the boundary layer. If the boundary layer is optically thick then the gas cools efficiently and so collapses quickly onto the white dwarf surface, forming a geometrically thin equatorial belt around the white dwarf. The luminosity emerges at the local blackbody temperature, which is of order 20 – 50 eV for the case where all the remaining accretion luminosity is radiated (Pringle 1977; see also Frank King and Raine 1992). Conversely, if the gas is optically thin then radiative cooling is much less efficient, the gas can be heated up to much higher temperatures before reaching equilibrium with radiative cooling and/or adiabatic expansion, giving temperatures of order ~ 10 keV. Since the optical depth of the accreting gas is strongly linked to the mass accretion rate this predicts that mainly EUVE/soft X-rays are expected from DN in outburst, while hard X-rays can be produced by DN in quiescence (Pringle and Savonijje 1979; Tylenda 1981; King and Shaviv 1985, Narayan and Popham 1993; Popham and Narayan 1995). A logical extension of this model is that the vertical density gradients in the disk could ensure that some fraction of the accreting material remains optically thin even in outburst, producing some hard X-ray emission, as observed (Patterson and Raymond 1985a; 1985b).

The resulting hard X-ray spectrum in both quiescence and outburst should certainly consist of multi-temperature components as the accreting gas must cool in order to settle onto the white dwarf photosphere. Thus the continuum should be characterised by continuous temperature distribution, with the contribution from each temperature component being weighted by its emissivity. However, in addition to this intrinsic hard X-ray continuum, there should also be a component formed from reflection of this spectrum from the illuminated white dwarf surface and/or accretion disk. The reflection albedo is energy dependent, as at low energies the scattering probability is decreased by photo-electric absorption, whereas at higher energies Compton downscattering and the reduction of the scattering cross-section deplete the number of photons reflected. This results in a broad spectral “bump”, centered around 20 keV, while the dependence on photo-electric absorption at low energies gives a pronounced feature at the iron K edge energy in the reflected spectrum and an associated Fe $K\alpha$ fluorescence line, both of which are a function of the ionization state and elemental abundances of the reflecting gas (e.g. Lightman & White 1988; George & Fabian 1991; Matt, Perola & Piro 1991). Such models have been applied to magnetic CV systems (Beardmore et al 1995; Done, Osborne and Beardmore 1995; Cropper, Ramsey and Wu 1996; van Teeseling, Kaastra and Heise 1996), but have not yet been extended to the non-magnetic systems.

A further possible distortion of the hard X-ray spectrum in DN is from complex absorption. P Cygni line profiles are seen in these systems in the UV SiIV, CIV and NV resonance lines, but only in outburst, when the accretion rate is high (see e.g. the recent review by Drew 1993). The mass loss rate and ionization structure in this wind is poorly known, but the models which have most success in matching the blueshifted UV absorption features are optically thick at soft X-ray energies (e.g. Mauche and Raymond 1987; Hoare and Drew 1991; 1993). Thus partially ionized absorption may play an important role in determining the observed soft X-ray spectrum in outbursting DN spectra,

though the wind declines rapidly after the outburst peak (Verbunt et al 1984), so this is unlikely to be important for the quiescent emission.

These spectral distortions will bias the results from simple thermal model fits to the data. This is important as recent exciting developments in accretion disk structure have attempted to include a self consistent description of the boundary layer emission. In the quiescent state the disk density is low, so local cooling may be inefficient enough that *radial* energy transport is also important. Numerical solutions by Narayan and Popham (1993) including these advected energy terms give predictions of the temperature-emissivity structure of the boundary layer. However, as both reflection and ionized absorption give an observed spectrum that is flatter than the intrinsic continuum, their neglect can give an overestimate of the amount of high temperature material.

SS Cyg is the brightest DN at in hard X-rays, so is the obvious candidate for detailed spectral studies. Here we analyse the available archival data from GINGA (2 spectra) and ASCA (1 spectrum). These show the system in three different states, quiescence, decline from a normal (fast rise) outburst, and in anomalous (slow rise) outburst, respectively. We evaluate the importance of reflection and partially ionized absorption, and so obtain the underlying intrinsic continuum temperature-emissivity distribution of the hot plasma. These data have been previously reported by Yoshida et al (1992), Ponman et al (1995) and Nousek et al (1994) but these authors only fit the spectra with simple thermal models. Here we include reflection and ionized absorption, and explicitly fit continuous temperature distribution models to the underlying intrinsic spectral shape.

We clearly detect the signatures of reflection in all the spectra. In outburst this is consistent with the hard X-ray emitting plasma forming a corona over the white dwarf, forming a reflection spectrum from both the white dwarf surface and inner disk. However, in quiescence there is significantly less reflection, which we interpret as indicating that the inner disk is disrupted or optically thin during quiescence. The ASCA data also show partially ionized absorption, as expected from the outflowing wind.

The abundances of the elements can be constrained, especially in the ASCA data. The line emission is significantly weaker than expected from solar abundances. We examine possible deviations from coronal equilibrium, but conclude that none of these can cause the observed line deficit. The high iron abundance relative to the other elements in the Anders & Grevasse (1989) ‘solar’ compilation is inconsistent with the data. Newer ‘solar’ abundance determinations (Grevasse, Noels & Sauval 1996) give a relative iron abundance much closer to the Morrison & McCammon (1983) values, which are similar to the elemental abundance ratios in the ASCA data presented here.

The underlying continuum is well described by a continuous (power law) temperature-emissivity distribution of hot material. In quiescence this is strongly weighted towards high temperatures, so that it is indistinguishable from a single temperature component. This is inconsistent with the expected cooling of hot gas. Either there is some reheating process or the cool components are masked by partial absorption, perhaps by an inner disk which is optically thin to electron scattering which photoelectrically absorbs the soft

X-ray emission from the boundary layer below the disk. By contrast, the outburst spectrum is dominated by cool components, and cannot be described by a single temperature plasma. While the emission is significantly softer, the total luminosity is similar to that in quiescence, assuming that the material cools down onto the photosphere.

2 THEORETICAL MODELS

2.1 Continuum Emission

If gas is heated up to some temperature T_{max} and then allowed to cool down to the photospheric temperature T_{bb} at constant pressure in a constant gravitational potential so that the luminosity is solely driven by the temperature drop then the resulting spectrum can be described by a sum of thermal spectra from T_{max} to T_{bb} such that

$$L(\nu) \propto \int_{T_{bb}}^{T_{max}} \frac{\epsilon(T, n^2, \nu)}{\epsilon(T, n^2)} dT$$

where $\epsilon(T, n^2, \nu)$ is the bremsstrahlung spectral emissivity and $\epsilon(T, n^2)$ is the total (integrated over ν) bremsstrahlung emissivity. More general *cooling flow* models include a weighting factor $(T/T_{max})^\alpha$ in the integrand (see e.g. Johnson et al 1992; Done et al 1995).

Explicit calculations of the emission from the boundary layer are extremely difficult due to the strongly shearing and probably turbulent nature of the flow. Any accretion disk problem is inherently two dimensional (at least) as the matter flow is radial while the energy is transported vertically (through radiation) as well as radially (through advection). Reducing the problem to 1 dimension by vertical averaging of the accretion disk structure (the standard Shakura–Sunyaev approach) makes the equations far more tractable. This is the approach used by Narayan & Popham (1993) and Popham & Narayan (1995) to calculate the temperature structure of the boundary layer. Their models then give the predicted temperature–emissivity distribution in the boundary layer. Figures 1a and b show spectra calculated from the models of Narayan & Popham (1993) for the quiescent emission for a white dwarf of mass $M = M_\odot$ and radius $R = 5 \times 10^8$ cm for a mass accretion rate of $\dot{M} = 10^{-9.5}$ and $10^{-10.5} M_\odot \text{ yr}^{-1}$, respectively. The dotted lines in these figures show a comparison with an $\alpha = 0$ cooling flow model of maximum temperature equal to that of the highest temperature emission present in the advective boundary layer model, which is 8.78 and 16.4 keV, respectively. The two models are remarkably similar at low \dot{M} , but begin to diverge at higher mass accretion rates. In outburst however, their models give no hot optically thin component to the emission (Popham & Narayan 1995), probably because of the limitations of the 1 dimensional approach whereas the hard X-ray emission is thought to be from material escaping from the boundary layer to form a corona over the white dwarf/disk.

Calculations in (at least) 2 dimensions are required in order to follow coronal structure. Kley (1989) and Hujeirat (1995) solve numerically a fully 2 dimensional set of (simplified) equations describing the hydrodynamic and thermal properties of the gas. The results of Kley (1989) are especially relevant as these include most of the white dwarf

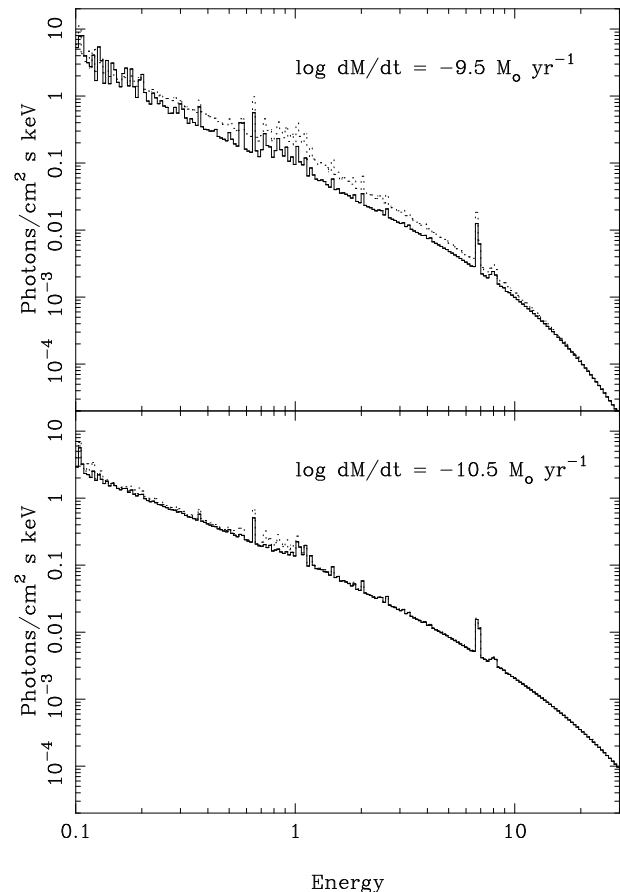


Figure 1. Spectra calculated from the models of Narayan & Popham (1993) for the quiescent emission from a $1M_\odot$ object accreting at $\log \dot{M} = -9.5$ (a: top panel) and $-10.5 M_\odot \text{ yr}^{-1}$ (b: lower panel) are shown by the solid lines. The dotted lines give the comparison spectrum expected from plasma of solar abundance heated to the same maximum temperature as in the Narayan & Popham (1993) models, cooling by radiation alone, at constant pressure in a constant gravitational potential. The models are very similar, especially at low mass accretion rates.

surface in the calculation, and so can follow any hot, optically thin gas which expands to form a corona around the white dwarf, while the grid used by Hujeirat (1995) only covers the equatorial belt of the white dwarf. Kley (1989) does indeed show that an optically thin, hot (~ 6 keV for his assumed system parameters) corona forms around the white dwarf and inner disk during outburst. The temperature and density contours can in principle be combined to give the temperature–emissivity distribution (which is the observed quantity) but in practice the published data plots are too complex to convert into this form so we cannot directly compare these calculations with the data.

However, even a two dimensional approach is probably not adequate, as this cannot describe oblique shocks in the plane of the disk which are perhaps the most likely outcome of the disk/star interaction. Even more seriously, all these models (both 1 and 2 dimensional) assume that the

viscosity in the boundary layer and the disk is produced the same mechanism (generally assumed to be turbulent convective motions) and so use the same parameterisation to describe the viscosity in both regions. This is at odds with recent results which show that convective turbulence transports angular momentum *inwards* not outwards as is required for accretion (Balbus, Hawley & Stone 1996), and that the magnetic dynamo models (Tout & Pringle 1992) based on the magnetohydrodynamic instabilities (Balbus & Hawley 1991) are the most likely source of the strong viscosity inferred for accretion disks. The viscosity in the boundary layer may then be very different from that in the disk since it is not at all obvious that the MHD dynamo can work outside of the ordered velocity field in the disk (since it uses Keplerian shear velocities to transform radial magnetic field to azimuthal, the Parker instability to transform azimuthal field into vertical, and the Balbus–Hawley instability to regenerate radial field from vertical. The dissipation required for viscosity then comes from magnetic field reconnection from opposing vertical field lines: Armitage, Livio & Pringle 1996).

2.2 Reflection from the White Dwarf Surface

The intrinsic continuum can be reflected by any optically thick material. The reflection models calculated to date have generally assumed the specific geometry of a (pointlike or extended) source illuminating a flat slab (Lightman and White 1988; Matt, Perola and Piro 1991; George and Fabian 1991; Zycki et al 1994; Magdziarz and Zdziarski 1995; Van Teesling et al 1996). Here the geometry of the boundary layer emission is more complex, as we expect that the X-ray emission will be produced in an equatorial belt around the white dwarf. The vertical extent of this belt is model dependent. The advective boundary layer models of Narayan and Popham (1993) have $h/r \sim 0.3 - 1$ (R. Popham, private communication), while King and Shaviv (1984) and Pringle and Savonije (1979) envisage the quiescent boundary layer as extending as a corona over the whole of the white dwarf surface. In outburst all the models agree that the optically thick boundary layer should be extremely compact both in height and in radial extent. However, the structure of the residual optically thin hard X-ray emission that can be seen in outburst is less clear, and such high temperature gas is again likely to expand adiabatically out of the equatorial plane before it cools (Pringle and Savonije 1979; King and Shaviv 1984). Thus we use the vertical extent of the boundary layer as a free parameter.

The radial extent of the boundary layer is observed to be very small, $\leq 1.15R_{WD}$, from eclipse mapping of the X-ray emission in the quiescent dwarf novae HT Cas (Mukai et al 1996). Interestingly, the width of the radiative boundary layer in the models of Narayan and Popham (1993) is $1.15R_{WD}$ for mass accretion rates of $\dot{M} = 10^{-9.5} M_{\odot} \text{ yr}^{-1}$, and *increases* for smaller mass accretion rates. This is in potential conflict with the data as the hard X-ray flux from HT Cas only requires an accretion rate of $\sim 2 \times 10^{-12} M_{\odot} \text{ yr}^{-1}$ (Mukai et al 1996), but the fractional contribution of the hard X-rays to the bolometric luminosity is highly uncertain and could be very small (Van Teeseling, Beuermann and Verbunt 1996). Here we follow the observations and assume that the boundary layer is thin in the radial direction.

The boundary layer emission will clearly illuminate the white dwarf surface, but the extent to which this can be seen depends on the accretion disk geometry. In outburst it is generally supposed that the disk is optically thick and has an inner radius which is very close to the white dwarf surface (e.g. Popham and Narayan 1995). However, there is considerable debate on the structure of the accretion disk during quiescence. Several models have suggested that there is no inner disk in quiescence, in order to explain the delay in the onset of the UV flux rise during outburst with respect to the optical (as seen by e.g. Mauche et al 1995). Meyer and Meyer–Hofmeister (1994) proposed that the inner disk could be evaporated by a coronal siphon flow; Livio and Pringle (1992) proposed that the inner disk formation during periods of low mass accretion rates was inhibited by low level ($B \sim 10^4 - 10^5$ G) magnetic fields, while Armitage et al. (1996) proposed that the inner disk is depleted by a magnetic wind. Alternatively, the inner disk may be present in quiescence, but not be optically thick. This is suggested by Mukai et al (1996) to explain the marginally narrower X-ray than optical eclipse ingress/egress width in HT Cas. If the accretion disk has a column of $\sim 10^{23-24} \text{ cm}^{-2}$ then it is optically thick to photoelectric absorption of the 2–3 keV flux (which dominates the ASCA countrate) emitted by the boundary layer below the disk but is optically thin to the optical emission from the white dwarf photosphere as long as the disk density is less than $\sim 10^{15-16} \text{ cm}^{-3}$ so that the free–free opacity is small. Thus we assume that an optically thick disk extends down to the boundary layer in outburst, but that in quiescence the inner disk *may* be disrupted or optically thin.

The proposed geometries are shown in Figure 2a and b. The boundary layer half thickness subtends an angle β at the center of the white dwarf, and the system is viewed at some inclination angle i (measured from the normal to the disk plane). The appendix shows that the reflection component from the white dwarf surface in SS Cyg, where $i = 37^\circ$ (Cowley et al 1980), can be approximated by that from an isotropically illuminated slab viewed at 60° , irrespective of β .

2.3 Reflection from the Disk

There should be an additional reflection spectrum from the optically thick disk if it does extend down to the inner boundary layer (see figure 2a). This is not so simple to quantify, firstly as the geometry is complex (the reflection spectrum from the region of the disk shadowed by the white dwarf cannot be seen by the observer) and secondly because the amount of reflection depends also on the distribution of incident photon angles, and is larger for large incident angles such as are predominantly expected here. Photons which skim along the surface of the disk have a large path length through the material. They are then absorbed/reflected in the upper layers of the disk, so it is very easy for any reflected photons to escape (e.g. George and Fabian 1991). There is also the problem that the reflector intercepts not just the intrinsic spectrum but also the reflection spectrum from the white dwarf surface. Thus we will just treat the limiting cases of an infinitely thin disk illuminated by a boundary layer with $\beta = 0$ and $\beta = \pi/2$. The former case is similar to that of a point source above a disk, as for each point on

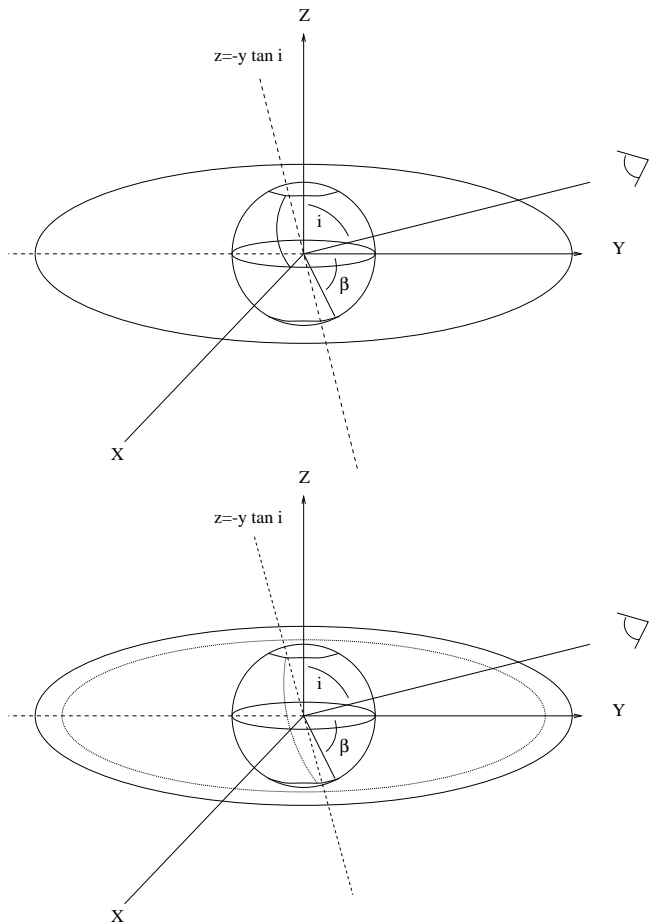


Figure 2. The assumed geometry of the boundary layer. The X-ray emission forms a corona over the white dwarf surface, extending up to an angle β towards the pole. The observer is assumed to be on the Y axis, viewing the system at some inclination i with respect to the normal to the accretion disk in the X-Y plane. In 'a' this disk is assumed to be optically thick all the way down to the boundary layer, whereas in 'b' the inner disk is either not present or is optically thin so that the emission from the boundary layer below the equatorial plane can also be seen

the boundary layer near the equator the emission is limited to a hemisphere pointing away from the white dwarf surface, and half of this will intercept the disk while the other half will not. Thus the effective solid angle subtended by the disk is $\Omega/2\pi = 1$. In the latter case, where the emission extends all the way up to the poles, the reflection spectrum normalisation is smaller. Radiation emitted at the poles is again confined to a hemisphere pointing away from the white dwarf surface but this does not intersect the disk at all, and so contributes only to the continuum emission rather than to the disk reflection. In fact the solid angle subtended by the disk to an optically thick X-ray emitting sphere is $\Omega/2\pi = 1/2$ (Chen and Halpern 1989), so as $\beta \rightarrow \pi/2$ the additional reflection component is then $0.5\times$ that expected from an isotropically illuminated disk viewed at inclination i . For SS Cyg the angles are such that an $\Omega/2\pi = 1/2$ disk reflection component viewed at 37° is almost identical (in shape and normalisation) to that from the white dwarf surface ($\Omega/2\pi = 1$) viewed at the mean angle of 60° , so the additional reflection spectrum expected from the inner disk

(if it exists) is $1 - 2\times$ that expected from a slab viewed at 60° .

3 OBSERVATIONS

SS Cyg was observed twice with GINGA (2–20 keV), once in quiescence (25–27 Nov 1987) and once during decline of a normal outburst (2–5 Dec 1990). The data were extracted in 64 second binning using standard selection criteria (maximum pointing offset from the source of 0.4° , soft electron rates of $\text{SOL} < 10$, magnetic rigidity between $7 \leq \text{COR} \leq 20$, surplus count rate above the upper discriminator of $\text{SUD} \leq 10$, and Earth elevation angle between $6 \leq \text{YELEV} \leq 120$).

The GINGA proportional counters are split into two separate layers, top and mid, where the mid layer is more sensitive above 15 keV, but has very little effective area below 8 keV (Turner et al 1989). The data mode chosen for the majority of both SS Cyg observations was MPC2, in which the top and mid layer are combined, rather than the usual faint source data mode of MPC1 where the mid layer spectra can be discarded to increase signal-to-noise. The standard 'universal' background subtraction technique, in which blank sky observations over a period of several months around the date of the observation are used to calculate the contribution from the diffuse cosmic X-ray background, particle background and the induced satellite radioactive decay components (Hayashida et al 1989; Williams et al 1992) is optimised for MPC1 mode data, so is not necessarily appropriate here. Also, SS Cyg is in the galactic plane ($b = -7$) so the spectrum at the lowest energies can also be contaminated by the diffuse galactic background. Instead we use a 'local' background (Williams et al 1992), where data from a nearby (in both time and galactic coordinates) were also extracted, using the same selection criteria as the source except that a larger range in geomagnetic parameters ($\text{SUD} \leq 14$) and offset angle ($\leq 0.5^\circ$) is allowed. This blank sky data is then used to model the background components in the source data. For the 1987 data the background observation is not sufficiently long to sample all the same background levels as seen during the source observation so we exclude parts of the SS Cyg observation with $\text{SUD} \geq 8$. Two nearby backgrounds were used to model the 1990 data as the background taken between the two main blocks of source data was noisy. Systematic errors induced by using only a short segment of background data are included by increasing the error bar on the background by a factor 1.5. This is a conservative procedure and probably results in the overly small values of χ^2 derived in Sections 4.1 and 4.2. The background subtracted data is then attitude corrected in order to produce the final dataset, and a systematic error of 0.5 per cent is added to take account of residual uncertainties in the determination of the instrument response.

The default (Rev 1) screened ASCA (0.6–10 keV) data for each instrument were taken from the archive. These were extracted with elevation angle $\geq 10^\circ$, geomagnetic rigidity $\geq 6 \text{ GeV}/c$, pointing within 0.01° of the target position, not in the South Atlantic Anomaly or in fine guidance mode. For the SIS data there is the further criteria that the bright Earth angle is $\geq 20^\circ$, and all faint mode data are converted to bright mode, and combined with the original bright mode

data. Source spectra for the SIS and GIS were extracted over a circle of radius 4 and 6 arcminutes, respectively, and background was taken from the same image as the source data. The effective area curve for each instrument was derived from the source position data and this, together with the standard response matrices (s0c1g0234p40e1_512v0_8i.rmf, s1c3g0234p40e1_512v0_8i.rmf, gis2v4_0.rmf, gis3v4_0.rmf) give the instrument response. The source data were then grouped to a minimum of 20 counts per bin so that χ^2 fitting is appropriate.

4 SPECTRAL FITTING

The data were fitted using the XSPEC spectral fitting package version 9.00 (Arnaud 1996). All error bars or upper limits quoted are $\Delta\chi^2 = 2.7$ (90 % confidence level for 1 free parameter). We caution that some parameters are strongly coupled (especially in the low spectral resolution GINGA data), so the allowed strengths of e.g. the Gaussian line and reflection continuum are strongly (anti)correlated. The equivalent widths of any additional Gaussian line components are quoted by re-evaluating the model on a dummy response matrix with 1000 energy grid points between 0.2 and 20 keV. This means that the 6.4 keV line is calculated with respect to the line-free continuum at 6.4 keV, whereas with the instrumental energy binning the 'continuum' can be contaminated by the hot plasma line emission. The interstellar column density to SS Cyg is fixed at $N_H = 3 \times 10^{19} \text{ cm}^{-2}$, as determined from the depth of narrow UV absorption lines seen against the bright outburst spectrum (Mauche, Raymond and Cordova 1988).

For single temperature hot plasma spectra we use the `mekal` model in XSPEC (see the XSPEC users manual for a complete description of the supported models), while for a power law emissivity-temperature distribution plasma we use a modification of the `cemek1` code in XSPEC, where the luminosity of each temperature component is weighted by a factor $(T/T_{\text{max}})^\alpha$. The code as released calculates the integral over temperature logarithmically, without modifying the step size from dT to $d \log T$. Thus the α produced by the code is 1 larger than the true weighting factor. In all that follows the α quoted is the XSPEC weighting factor. Numerically the code also had to be modified by changing the order of integration (starting with the highest temperature component rather than the lowest) so that the spectrum changes smoothly with changing T_{max} . The density in both plasma codes is fixed at $n = 1 \text{ cm}^{-3}$. Reflection of the continuum spectrum is calculated from the code of Magdziarz and Zdziarski (1995), with the inclination angle fixed at 60° as appropriate for SS Cyg (see section 2), but with the fractional contribution left as a free parameter. All these models assume that the abundances with respect to H of all the elements scale together, and that this fractional abundance relative to the Solar determination of Anders and Gervasse (1989) is a free parameter. The iron fluorescence line that should accompany the reflection continuum is included as a separate narrow Gaussian, with line energy of 6.4 keV being appropriate for a mainly neutral reflector. These four model components (single temperature plasma, power law temperature-emissivity distribution plasma, reflection con-

tinuum and Gaussian emission line) are denoted by T, pIT, R and g respectively in all the tables.

There is also the possibility of complex absorption. In quiescence the inner disk may be present but be optically thin to electron scattering (section 2.2). This may give rise to partial absorption of the X-ray emission. The fraction of the emission that is occulted by the inner disk can be derived from the difference in the emitting area observed with and without a disk (i.e. the difference in normalisation factors in equations 1 and 2 of the appendix). For SS Cyg at an inclination of 37° this gives rise to a maximum expected covering fraction of 0.5 if the boundary layer is concentrated in the equatorial plane ($\beta \rightarrow 0$) or a minimum covering fraction of 0.2 for $\beta \rightarrow 90^\circ$. We assume that the optically thin disk is neutral and model this by the `pcf` code in XSPEC. The partially ionized absorption expected in outburst from transmission of the X-ray spectrum through the outflowing wind is modeled by the `absori` code in XSPEC. The ion populations are found by balancing the temperature dependent dielectronic and radiative recombination rates against photoionization as in Done et al (1992). The thermal balance equations are not calculated self consistently. Instead the temperature of the material is fixed at $5 \times 10^4 \text{ K}$, as appropriate for the derived low ionization states (see section 4.3 and e.g. Kallman and McCray 1982 figures 21 and 22). The code assumes that the ionization balance is determined by a power law X-ray spectrum. The continuum from SS Cyg can be roughly characterised by a power law of photon index $\Gamma = 2$ in outburst and $\Gamma = 1.8$ in quiescence, so we fix the index at the relevant value for each spectrum. Model calculations of the ionization state of the wind have tended to concentrate on photoionization by the putative boundary layer blackbody emission but the harder X-ray emission will also contribute to the ionization balance. This especially important in determining the abundances of the ions which absorb in the X-ray bandpass, such as OVII. Both absorption models use the fixed abundances of Morrison & McCammon (1983) and are denoted by `pcf` and `pia` respectively in all the tables.

4.1 GINGA 2–20 keV Spectrum (1987): Quiescence

Results from all the spectral fits in this section are detailed in table 1. Since these data are the same as those used by Yoshida et al (1992) we first check for consistency by using their model of a bremsstrahlung spectrum with narrow Gaussian emission line. This gives a good fit to the data ($\chi^2_\nu = 15.3/22$), with derived continuum and line parameters which are consistent with those quoted by Yoshida et al (1992). However, a bremsstrahlung spectrum is physically unlikely as there will be elements other than just pure hydrogen in the accreting material. Thus we replace this *ad hoc* continuum and line with a hot plasma spectrum in which the line emission is calculated self consistently, and fix the absorption at the interstellar value. This gives a poor fit to the spectrum, with $\chi^2_\nu = 39.6/24$ for a temperature of $15.2 \pm 0.7 \text{ keV}$ and abundance of 0.71 ± 0.10 . Including a second temperature component, as has often been suggested (Yoshida et al 1992; Nousek et al 1994) does not give a significantly better fit ($\chi^2_\nu = 32.6/22$ for $kT_1 = 9.2^{+2.9}_{-3.0} \text{ keV}$ and $kT_2 = 57^{+43}_{-37} \text{ keV}$). Adding further separate temperature

components does not result in any significant improvement in the fit.

Such *ad hoc* multi-temperature models can approximate the spectrum of a continuous temperature distribution. A power law temperature-emissivity distribution hot plasma model gives a fit which is not significantly different ($\chi^2_\nu = 37.6/23$) from the single temperature description, with the data requiring that the most weight is given to the higher temperature components ($\alpha \geq 1.6$).

As the theoretical continuum spectral shape is not known *a priori* we are justified in trying an arbitrary emissivity/temperature relation. One such model describes the differential emission measure, $\phi(T)$, as an exponential function of an k th order Chebyshev polynomial, $P_k(T)$, such that $\phi(T) \propto \exp(\Sigma a_k P_k(T))$ (Lemen et al. 1989), where the exponential function ensures positivity. We modified the `cp6mk1` model in XSPEC so that the maximum temperature was a free parameter rather than being fixed at 10 keV, redefined the Chebyshev polynomial coefficients to a more standard form (e.g. Press et al 1988), and again reversed the order of integration. Fitting with this model resulted in a $\chi^2_\nu = 33.0/18$, similar to that from the two temperature plasma description. The derived emissivity distribution has two peaks at similar temperatures to those found in the two temperature model so we do not tabulate the results of this fit.

All the above plasma models give systematic residuals at the iron line and edge energy. These are shown in figure 3 for the best fitting two temperature plasma model, and are very suggestive of the presence of a reflection continuum and its associated iron $K\alpha$ line emission. Including an additional cold iron line to even the single temperature plasma model gives a highly significant reduction in χ^2_ν to 15.0/23. This line should also be accompanied by a reflection continuum, but the strength and shape of this continuum is dependent on the elemental abundances and ionization state of the reflector as well as the geometry of the source with respect to the reflector and the inclination of the reflector with respect to the observer (see Section 2). We fix the inclination at 60° , and constrain the abundances in the reflector to be equal to those of the hot plasma. This gives only a marginal improvement in the fit, with $\chi^2_\nu = 13.2/22$ compared to the 6.4 keV line fit described above, but physically it gives a coherent picture of the source as the amount of 6.4 keV fluorescent line is then consistent with a reflection origin.

Replacing the single temperature continuum model with a power law temperature-emissivity distribution and fitting this, together with its reflection spectrum and a cold iron line as above, gives no significant improvement in the fit ($\chi^2_\nu = 12.2/21$), with the incident spectrum being weighted towards the high temperature components ($\alpha \geq 1.5$). The total intrinsic 25eV–100 keV flux in this model is 1.2×10^{-10} ergs cm^{-2} s^{-1} , which gives a bolometric luminosity of the optically thin gas of 1.4×10^{32} ergs s^{-1} assuming a distance of 100 pc (Bailey 1981). This implies a *minimum* mass accretion rate of $\dot{M} = 10^{-10.4} M_\odot \text{yr}^{-1}$ assuming that the mass of the white dwarf is $0.8 M_\odot$ (Cowley et al 1980) and its radius is $R_{WD} = 7 \times 10^8$ cm (Nauenberg 1972). The temperature-emissivity distribution derived from the data is inconsistent with the $\alpha = 1$ gas cooling model and the advective boundary layer model at these accretion rates (see Figure 1), while freezing α at unity gives significant excess emission at low

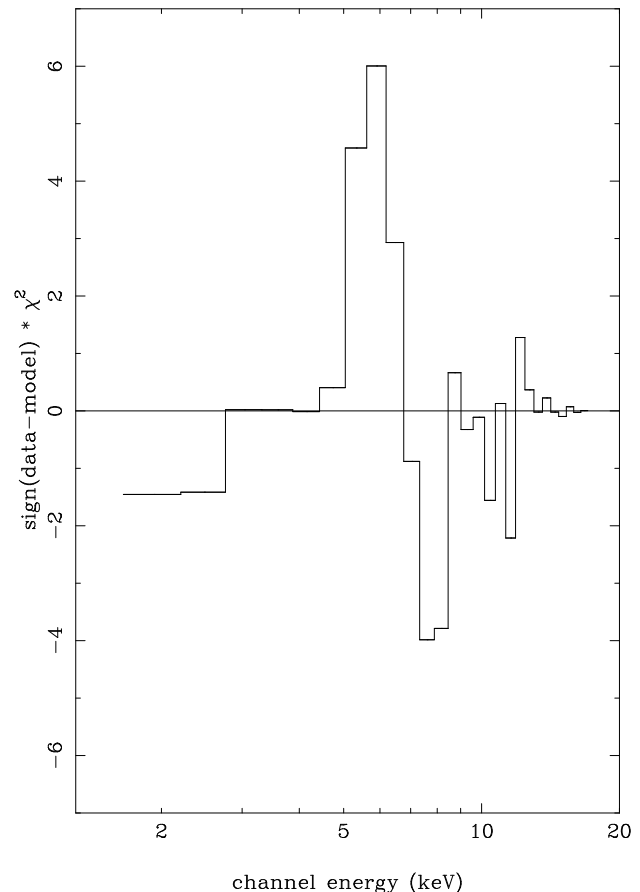


Figure 3. The χ^2 residuals of the GINGA quiescent spectrum to a two temperature plasma model. There is an excess at ~ 6.4 keV, together with a decrement at 7-8 keV. These features are consistent with the iron fluorescent line and edge expected from reflection in cold material.

energies. The mass accretion rate given above may be underestimated by its neglect of possible optically thick emission from the boundary layer, but such corrections are likely to be small as the optically thick emission in quiescence seems to be weak (Ponman et al 1995). One possible way for the spectra to be made consistent with these models is to add in excess absorption. The data clearly are already well fit statistically but the addition of partial covering by cold material with the absorbed fraction fixed at 0.2 (see Section 3) gives an excellent fit ($\chi^2_\nu = 10.2/20$) for a column of $N_H \sim 2 \times 10^{22}$ cm^{-2} with the derived temperature-emissivity relation fixed at $\alpha = 1$.

Alternatively, the excess absorption can be described by complete covering by partially ionized material (the `absori` model in XSPEC with the power law index fixed at 1.8). Again, this gives a good fit ($\chi^2_\nu = 10.3/20$) with the $\alpha = 1$ continuum model for a column of $N_H \sim 5 \times 10^{21}$ cm^{-2} . Both absorption models increase the intrinsic (absorption corrected) 25eV–100 keV flux to 1.4×10^{10} ergs cm^{-2} s^{-1} .

Table 1. Quiescent (GINGA) data

model	kT ^a (keV)	A	N ^b	α	R	EW (eV)	N _H ^c	ξ^d	χ^2_ν
1T	15.2 ± 0.7	0.71 ± 0.10	4.1 × 10 ⁻²						39.6/24
2T	9.2 ^{+2.9} _{-3.0}	0.69 ^{+0.14} _{-0.09}	2.7 × 10 ⁻²						32.6/22
	57 ⁺⁴³ ₋₃₇		1.7 × 10 ⁻²						
pIT	19.7 ^{+5.7} _{-4.8}	0.74 ± 0.11	0.20	2.8 ^{+∞} _{-1.2}					37.6/23
1T+g	15.6 ± 0.7	0.42 ± 0.13	4.3 × 10 ⁻²			170 ± 60			15.0/23
1T+R+g	13.0 ^{+3.0} _{-2.3}	0.35 ^{+0.15} _{-0.10}	4.2 × 10 ⁻²		0.5 ^{+0.7} _{-0.5}	125 ⁺⁹⁵ ₋₉₀			13.2/22
pIT+R+g	15.4 ^{+8.8} _{-5.4}	0.35 ^{+0.16} _{-0.11}	0.21	2.9 ^{+∞} _{-1.4}	0.6 ^{+0.9} _{-0.6}	100 ⁺⁹⁰ ₋₈₅			12.2/21
pcf(pIT+R+g) ^e	21 ⁺¹¹ _{-5.7}	0.38 ^{+0.16} _{-0.11}	0.10	1 ^f	0.6 ^{+1.0} _{-0.6}	85 ⁺¹⁰⁰ ₋₈₅	16 ⁺¹⁷ ₋₇	0 ^e	10.2/21
pia(pIT+R+g)	21 ⁺¹¹ _{-5.8}	0.38 ^{+0.17} _{-0.11}	0.10	1 ^f	0.6 ^{+1.1} _{-0.6}	85 ⁺⁹⁰ ₋₈₅	4.7 ⁺³⁶ _{-3.5}	18 ⁺¹⁰⁰⁰ ₋₁₈	10.3/20

^a This is the maximum temperature in the pIT models

^b The normalisation of the plasma model in units of 10⁻¹⁴/(4πD²) × Emission Measure

^c Units of 10²¹ cm⁻²

^d Defined as L/nr² where r is distance from material of density n illuminated by a source of luminosity L

^e Covering fraction fixed at 0.2

^f Parameter fixed

4.2 GINGA 2–20 keV Spectrum (1990): Decline from Normal Outburst

These data were reported by Ponman et al (1995), who noted that the spectrum is significantly fainter and softer than that seen in quiescence. They split the observation into two sections in order to compare them with simultaneous ROSAT survey data. However, they noted that there was no significant change in hard X-ray spectral shape between the two segments, even though the softer ROSAT data, which are dominated by a separate low temperature component, show substantial variability. Thus here we co-add all the data to get maximum signal to noise. A single temperature bremsstrahlung continuum and (broad) Gaussian emission line gave results consistent with those of Ponman et al (1995).

We test the same series of models as described above, and details of all the spectral fits are given in table 2. Again, neither single nor multiple temperature models give a good fit to the continuum. However, unlike the quiescent data, adding a 6.4 keV iron emission line to the single temperature continuum does not produce a statistically acceptable fit to the data. Similarly, a single temperature continuum together with a reflection continuum and line fails to fit the data ($\chi^2_\nu = 51.1/22$). A good phenomenological description of the data can only be achieved by adding a 6.4 keV emission line to an intrinsically multi-temperature continuum, such as a two temperature model ($\chi^2_\nu = 19.0/21$), or a continuous power law temperature-emissivity distribution ($\chi^2_\nu = 18.4/22$). The lower value of the temperature weighting index α in this latter fit indicates the much softer spectrum seen in outburst compared to that in quiescence.

Since the continuous temperature distribution seems more physically likely as well as giving a better fit to the data we use this as our intrinsic spectrum and include its corresponding reflection continuum in the fit as well as the 6.4 keV line emission. This gives a significant reduction in χ^2_ν to 12.2/21, so that in these data the reflection continuum itself is detected separately from the line emission. The model here assumes that the reflecting material is neutral, so that the reflected edge is at 7.1 keV. This is at first sight incom-

patible with the results of Ponman et al (1995), where the fitted edge energy of 8.3 keV implied highly ionized material. However, with the limited resolution of GINGA, the derived energy of spectral features is strongly dependent on the assumed continuum form (see e.g. Beardmore et al 1995 for a similar example of this effect),

Including a warm absorber (with illuminating power law index fixed at $\Gamma = 2$) does not result in a significant improvement to the fit ($\chi^2_\nu = 10.2/19$). We do not tabulate the results of this fit as the parameters of the partially ionized column are largely unconstrained. The intrinsic (absorption corrected) 25eV-100 keV flux is 6.8×10^{-10} ergs cm⁻² s⁻¹ and 5.2×10^{-11} ergs cm⁻² s⁻¹ for models with and without ionized absorption, respectively.

4.3 ASCA 0.6–10 keV Spectrum (1990): Anomalous Outburst

We fit all 4 ASCA datasets simultaneously, and full details of the derived parameters are given in table 3. The overall shape is similar to that of the GINGA decline from outburst data, i.e. much softer and fainter than the quiescent spectrum in the 2–10 keV band. As shown by Nousek et al (1994), neither a single temperature plasma nor two plasma components give a good description of the spectrum, with $\chi^2_\nu = 3799/1159$ and 1331/1157, respectively. A three temperature model is required in order to give a statistically acceptable fit ($\chi^2_\nu = 1145/1155$). A continuous (power law) temperature-emission measure distribution gives an even better fit for fewer free parameters, with $\chi^2_\nu = 1117/1158$. This result is contrary to the assertion of Nousek et al (1994) that the lack of intermediate temperature plasma lines indicates that the emission measure – temperature distribution is not monotonic. The apparent discrepancy is probably due to their their assumption of solar abundances which led them to expect large line equivalent widths from any intermediate temperature components, while the line-to-continuum ratios in the data are a factor 2 weaker than predicted for solar abundance models. Their preferred phenomenological model fit to the data is a three temperature plasma, in which two

Table 2. Decline from normal outburst (GINGA) data

model	kT ^a (keV)	A	N ^b	α	R	EW (eV)	χ _ν ²
1T	6.9 ± 0.3	0.71 ± 0.08	1.34 × 10 ⁻²				73.5/24
2T	4.6 ± 0.6	1.0 ^{+0.18} _{-0.13}	1.13 × 10 ⁻²				46.0/22
	100 ^{+∞} ₋₇₀		3.18 × 10 ⁻³				
pIT	12.5 ^{+2.8} _{-2.1}	0.94 ± 0.13	3.05 × 10 ⁻²	1.00 ^{+0.54} _{-0.32}			55.1/23
1T+g	7.1 ^{+0.3} _{-0.4}	0.42 ± 0.12	1.39 × 10 ⁻²			240 ⁺¹¹⁰ ₋₁₀₀	52.6/23
1T+R+g	6.4 ^{+0.9} _{-0.7}	0.41 ± 0.11	1.39 × 10 ⁻²		0.5 ^{+0.8} _{-0.5}	180 ⁺¹³⁰ ₋₁₀₅	51.1/22
2T+g	1.15 ^{+2.0} _{-0.64}	0.41 ^{+0.21} _{-0.14}	5.2 × 10 ⁻³			350 ⁺¹⁴⁰ ₋₁₂₀	19.0/21
	8.6 ^{+0.9} _{-0.9}		1.2 × 10 ⁻²				
pIT+g	16.4 ^{+4.7} _{-3.3}	0.50 ^{+0.16} _{-0.15}	2.21 × 10 ⁻²	0.51 ^{+0.35} _{-0.25}		340 ⁺¹¹⁰ ₋₁₀₀	18.4/22
pIT+R+g	9.6 ^{+3.4} _{-1.7}	0.35 ^{+0.13} _{-0.09}	2.34 × 10 ⁻²	0.43 ^{+0.41} _{-0.38}	2.2 ^{+1.8} _{-1.5}	200 ⁺¹³⁰ ₋₁₂₀	12.2/21

^a This is the maximum temperature in the pIT models

^b The normalisation of the plasma model in units of 10⁻¹⁴/(4πD²) × Emission Measure

of the components are assumed to have solar abundances, while the third has zero abundance (a bremsstrahlung spectrum). The latter component acts as a means to dilute the strong line emission predicted by the other two temperature components.

There is strongly significant additional low-ionization iron line emission. Including a narrow Gaussian emission line at 6.4 keV in the fit gives a reduction in χ_ν² to 1077/1157, with line equivalent width of ~ 140 eV. However, including the reflection continuum that is expected to accompany such line emission does *not* lead to a decrease in χ_ν². The best fit reflected fraction is close to zero, with an upper limit of R ≤ 0.7, too small to produce the observed 6.4 keV emission line.

The low energy bandpass of ASCA means that these data are also sensitive to details of the absorption column along the line of sight, and physically some X-ray absorption should be present from the partially ionized wind seen in SS Cyg in outburst. The observed X-ray continuum spectrum can be described as a power law of photon index Γ ~ 2, so we use the model `absori` in XSPEC, with the photon index fixed to this value. This leads to a highly significant decrease in χ_ν² to 1024/1154 for N_H = 2.6 × 10²¹ cm⁻² at an ionization parameter of ξ = 1.4 for a fixed temperature of 5 × 10⁴ K. The underlying continuum form also changes, weighting the power law emissivity-temperature distribution even more towards the low temperature components, with α = 0.08, and the result is that the reflection component is now significantly detected, with R = 1.3. Models with the ionized absorption and 6.4 keV Gaussian line but without the reflection continuum give χ_ν² = 1036/1155. Thus the reflection continuum is significantly detected in these data, but only when the intrinsic continuum form is properly modeled.

The absorption in this partially ionized material has some effect on the derived bolometric luminosity of the X-ray emitting gas. Assuming that material cools down to the photospheric temperature of ~ 25 eV (Ponman et al 1995) gives a total flux from the hot plasma of 5.2 × 10⁻¹¹ ergs cm⁻² s⁻¹ (25 eV– 100 keV), while correcting for the ionized absorption increases this to 6.1 × 10⁻¹¹ cm⁻² s⁻¹, and further correcting for the interstellar column gives a flux of 11 × 10⁻¹¹ ergs cm⁻² s⁻¹. This is almost identical to the (absorption corrected) hot plasma flux seen in the GINGA

quiescent data integrated over the same band, showing that it is not necessarily true that there is less emission from the optically thin plasma in outburst, only that it is substantially softer.

The spectral resolution and sensitivity of ASCA make it possible to investigate the abundances of the elements in the hot plasma emission separately rather than assuming that they all scale together. We replace the plasma emission model with one in which the abundance of each element is a free parameter (the `cevmk1` model in XSPEC, modified as described in Section 4). The reflection abundance ratios are assumed to be solar, but the overall elemental abundance is a free parameter. This is fit separately from the plasma abundances as the plasma line emission may be distorted from that expected from coronal conditions (see section 5.1). Allowing the plasma iron abundance to be free relative to the other elements gives a significantly better fit (χ_ν² = 999.9/1152, for A_{Fe} ~ 0.3, A_{rest} ~ 0.5). Progressively fitting for the abundance of Si and S (which are the next strongest expected lines) gives χ_ν² = 978.7/1151 and 973.2/1150, for A_{Fe} = 0.28, A_{Si} = 0.72, A_S = 0.68 and A_{rest} = 0.41 (see table 4). A model in which all the other observable elements (O, Ne, Na, Mg, Al, Ar, Ca, Ni) are free gives χ_ν² = 964.2/1143 (C and N are fixed at solar as their Kα lines are below 0.6 keV so their abundance cannot be usefully constrained). Thus, from fitting coronal equilibrium models (together with the reflection continuum and line and ionized absorption), the data *require* that the elemental abundances are not solar and that the abundances ratios are not solar either. The model with fewest parameters that can describe the data (where adding in extra elemental abundance parameters does not significantly improve the fit), is one in which all the elements are tied together except for Fe which is a free parameter, and Si and S, which are tied to each other. This gives χ_ν² = 973.4/1151, for A_{Fe} ~ 0.3, A_{Si,S} ~ 0.7 and A_{rest} ~ 0.4. The spectrum was then truncated above 1.7 keV, so that the abundance of iron can be measured separately from the iron L complex. The contribution from reflection (continuum and line) can then be ignored, and the continuum parameters kT_{max} = 14.0, α = 0.15 and A_{Si,S} = 0.70 were frozen at their best fitting value above. This gives χ_ν² = 244.8/221 for A_{Fe} = 0.30 and

Table 3. Anomalous Outburst (ASCA) data

model	kT^a (keV)	A	N^b	α	R	EW (eV)	N_H^c	ξ^d	χ^2_ν
1T	$3.43^{+0.10}_{-0.06}$	$0.21^{+0.05}_{-0.02}$	3.0×10^{-2}						3799/1159
2T	$0.67^{+0.03}_{-0.01}$	0.51 ± 0.06	3.4×10^{-3}						1331/1157
	5.45 ± 0.07		2.2×10^{-2}						
3T	$0.56^{+0.04}_{-0.09}$	0.44 ± 0.06	2.8×10^{-3}						1145/1155
	1.10		3.0×10^{-3}						
	6.64		2.0×10^{-2}						
plT	18.2 ± 1.7	$0.48^{+0.06}_{-0.05}$	3.1×10^{-2}	0.47 ± 0.05					1117/1158
plT+g	$17.5^{+2.0}_{-1.5}$	$0.44^{+0.06}_{-0.05}$	3.1×10^{-2}	0.45 ± 0.06		140 ± 40			1077/1157
plT+R+g	$16.9^{+2.1}_{-3.2}$	$0.44^{+0.06}_{-0.07}$	3.2×10^{-2}	$0.46^{+0.06}_{-0.05}$	$0.08^{+0.58}_{-0.08}$	140 ± 40			1077/1156
pia(plT+R+g)	$12.6^{+3.6}_{-2.6}$	0.32 ± 0.05	2.5×10^{-2}	0.08 ± 0.11	1.3 ± 0.7	130 ± 40	$2.6^{+0.7}_{-0.6}$	1.4 ± 0.3	1024/1154
pia(plT+g)	$19.4^{+3.4}_{-2.4}$	0.41 ± 0.06	2.4×10^{-2}	$0.16^{+0.09}_{-0.11}$		160 ± 40	2.1 ± 0.6	$1.3^{+0.5}_{-0.3}$	1036/1155

^a This is the maximum temperature in the plT models

^b The normalisation of the plasma model in units of $10^{-14}/(4\pi D^2) \times$ Emission Measure

^c $\times 10^{21} \text{ cm}^{-2}$

^d Defined as L/nr^2 where r is distance from material of density n illuminated by a source of luminosity L

$A_{\text{rest}} = 0.42$, showing that the iron L complex is consistent with the iron K line strengths.

The abundances in the reflector are harder to quantify, since they correlate with the amount of reflection (e.g. George & Fabian 1991). However, the observed 6.4 keV line emission is also dependent on the abundances in the reflector and so provides an additional constraint. This is not straightforward, as the iron line equivalent width depends on the abundances of *all* the elements, not just iron, as the other elements provide opacity to the escaping iron line photons (George & Fabian 1991). The functional dependence is also made more complicated by the fact that the reflected line equivalent width also depends on the spectral shape of the illuminating continuum, as for hard spectra there is relatively more luminosity above the iron K edge that can be absorbed to produce the $K\alpha$ line. However, knowing a line equivalent width from one particular illuminating spectrum we can scale this by the ratio of the absorbed luminosity above the iron K edge to estimate the line equivalent width produced from reflection of any other spectral shape (Basko 1978). The abundance effects can then be estimated from George & Fabian 1991, who show that for Morrison & McCammon (1983) abundance ratios then the line equivalent width scales roughly as $A_{\text{all}}^{0.2}$ for $A_{\text{all}} \leq 1$, and that a relative over- or under-abundance of iron then gives a roughly proportional change in the line equivalent width.

The iron line has an angle averaged equivalent width of 110 eV with respect to a power law *illuminating* continuum of photon index $\Gamma = 1.9$ for Morrison & McCammon (1983) solar abundances (George & Fabian 1991). However, we are using Anders & Grevasse (1989) abundances, in which the iron abundance is $1.5\times$ larger than in Morrison & McCammon (1983), while all the other abundances are about the same. Thus with the Anders & Grevasse (1989) abundances we predict a line which is $1.5\times$ larger than this (Reynolds, Fabian & Inoue 1996), i.e. an equivalent width of 1.7 keV with respect to the reflected continuum. The ASCA spectrum of SS Cyg has best fit spectral parameters of $kT = 14$ keV, $\alpha = 0.15$, which has $0.81\times$ fewer photons that can be absorbed by the iron K edge than the $\Gamma = 1.9$ power law, so

predicting a line of 1.4 keV equivalent width with respect to the reflected continuum. If the abundance ratios in the reflector scale together then for $A_{\text{all}} \sim 0.3$ the line equivalent width is reduced by a factor ~ 0.79 , i.e. 1.1 keV. This is in strong contrast to the best fit model above (where the line and continuum from reflection are fit separately) in which the iron line equivalent width with respect to the reflection continuum is ~ 0.6 keV. Fitting a reflection continuum in which the reflector abundances scale together with self consistent line emission leads to a strong increase in χ^2_ν to 979/1152 (i.e. $\Delta\chi^2$ of 6, compared to the fits in which the line normalisation is free) for an incident continuum in which the abundances in the hot plasma are all tied together except for Fe, and Si and S which are tied to each other. This is a strong indication that the iron abundance in the *reflector* is too high with respect to the abundance of the other elements. The line is only consistent with that observed if the iron abundance in the reflector is subsolar in its ratio with respect to the other elements, and by an amount similar to that seen in the hot plasma line emission i.e. $A_{\text{Fe}} \sim 0.3$ while $A_{\text{rest}} \sim 0.5$.

We replace the Anders & Grevasse (1989) 'solar' abundances with those of Morrison & McCammon (1983), which has a factor 1.5 lower iron abundance (see section 5.2), in both the plasma and reflection codes. Details of some of these fits are given in Table 5. We first allow the line to scale independently of the reflection continuum, and the reflection spectrum abundances to scale independently of the hot plasma. With the abundance ratios tied at the (new) solar values we get $\chi^2_\nu = 1006/1153$ with $A \sim 0.4$. There is a marginally significant change in the fit if the Fe abundance is fit separately, with $\chi^2_\nu = 1002/1152$. However, this is driven by the relative overabundance of Si, and when Si is also free fit is significantly better with $\chi^2_\nu = 978.7/1151$ and the resulting Fe abundance is consistent with that of the rest of the elements. There is a further (marginally) significant decrease in χ^2_ν to 973.6/1150 with S free to vary, but no other significant deviations from (new) solar element ratios. In particular, allowing the abundance of O to be free gives $\chi^2_\nu = 973.4/1149$ for $A_O = 0.42^{+0.20}_{-0.16}$. The model with fewest

Table 4. Abundances with respect to Anders & Grevasse (1989)

kT^a (keV)	A (plasma)	α	A (reflector)	R	EW (eV)	N_H^b	ξ^c	χ_ν^2
$13.9_{3.4}^{+6.2}$	Fe= $0.29_{-0.05}^{+0.07}$ Si= $0.70_{-0.13}^{+0.15}$ S= $0.65_{-0.18}^{+0.21}$ rest= 0.40 ± 0.11	0.15 ± 0.11	$0.5_{-0.25}^{+0.75}$	1.9 ± 0.9	110 ± 30	$1.2_{-0.3}^{+0.5}$	$0.18_{-0.18}^{+0.30}$	973.2/1150

^a Maximum temperature in the plT models

^b $\times 10^{21} \text{ cm}^{-2}$

^c Defined as L/nr^2 where r is distance from material of density n illuminated by a source of luminosity L

parameters that describes the data is then one in which Si and S are tied together, but are free to vary from the Morrison & McCammon (1983) solar ratios ($\chi_\nu^2 = 974.9/1152$, for $A_{Si,S} = 0.65$, $A_{rest} = 0.37$). The predicted iron line equivalent width with respect to the reflection spectrum is then ~ 0.7 keV for $kT = 14$ and $\alpha = 0.15$. This is a much better description of the fluorescent line seen in the data than that expected from the Anders & Grevasse (1989) abundances. We set the reflector abundances to be equal to A_{rest} , and include the self-consistent line emission in the reflection spectrum, which gives a good fit at $\chi_\nu^2 = 976.7/1154$.

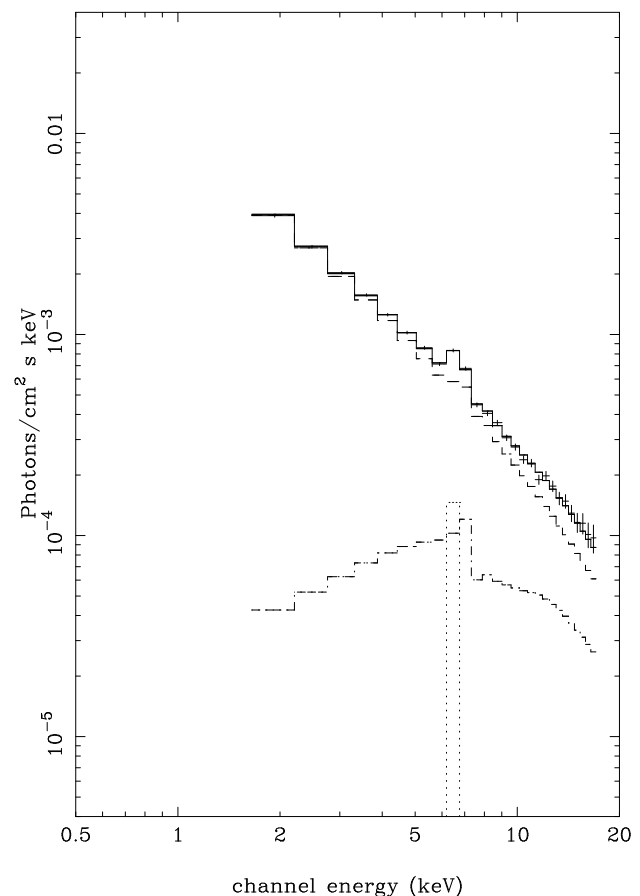
4.4 All Data

We fit a power law temperature–emissivity plasma model with Morrison & McCammon (1983) abundances, together with its reflection spectrum (also assuming these abundances) and a separate Gaussian line to all the data simultaneously, with the abundances tied across all the datasets. An ionized absorber is included for the ASCA data, and the plasma emission and Gaussian line normalisations, the maximum temperature and temperature weighting index are free to vary between the spectra. This gives an excellent $\chi_\nu^2 = 998.5/1197$, showing that the elemental abundances are consistent across all the datasets, with $A_{Si,S} = 0.64$ and $A_{rest} = 0.40$. The two outburst spectra are consistent with having the same amount of reflection, with no increase in χ_ν^2 when the two parameters are tied together, so that $\chi_\nu^2 = 998.5/1198$ for $R = 2.2$ in outburst and $R = 0.7$ in quiescence. This difference between the amount of reflection in outburst and quiescent is highly significant: tying all the reflected fractions together leads to an increase in χ^2 of 6.6.

The best fit model spectra for the quiescent, GINGA decline from outburst and ASCA outburst data fit simultaneously are shown in Figures 4, 5 and 6, respectively. The plasma parameters are $\alpha = 3.9, 0.8, 0.19$, and $kT_{max} = 13, 8.5, 12$, respectively, again showing that most of the gas is hotter in quiescence than in outburst.

5 DISCUSSION

All the data strongly require that the line emission is substantially weaker than expected from a coronal plasma with solar abundances. While this could simply indicate that the elements are subsolar, we first examine alternative possibilities.

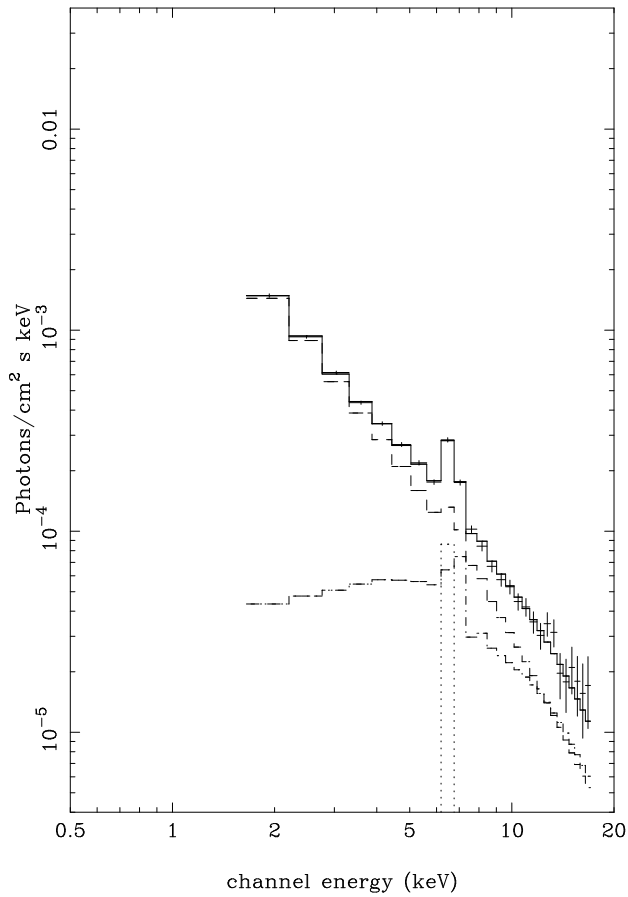

Figure 4. The best fit GINGA quiescent spectrum.

5.1 Validity of the Coronal Approximation

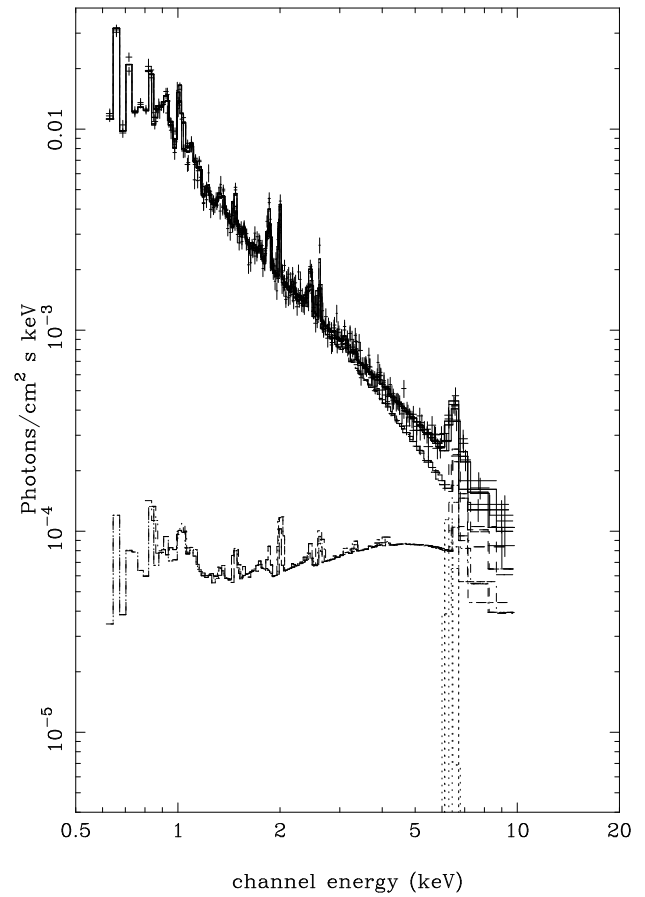
The data have been fit with coronal plasma models, which assume that radiative (and dielectronic) transitions are the dominant recombination processes balancing collisional ionization. All these processes involve only one electron in a free–bound (or bound–free) transition, so the resultant ion populations are independent of the electron density to first order. Most of the ions are in the ground state as the recombination rates are generally very much larger than the collisional ionization rates. However, at high densities colli-

Table 5. Abundances with respect to Morrison & McCammon (1983)

kT ^a (keV)	A (plasma)	α	A (reflector)	R	EW (eV)	N_H^b	ξ^c	χ^2_ν
$16.5^{+5.6}_{-4.3}$	$0.42^{+0.09}_{-0.06}$	0.11 ± 0.11	$0.9^{+4.1}_{-0.5}$	$1.5^{+0.9}_{-0.7}$	120 ± 40	1.6 ± 0.6	$0.7^{+0.4}_{-0.5}$	1006/1153
$13.9^{+6.2}_{-3.9}$	Fe= $0.39^{+0.09}_{-0.08}$ Si= $0.69^{+0.18}_{-0.16}$ S= $0.58^{+0.18}_{-0.17}$ rest= $0.38^{+0.11}_{-0.10}$	0.17 ± 0.11	$0.5^{+1.1}_{-0.25}$	1.9 ± 0.9	120 ± 40	$1.0^{+0.6}_{-0.4}$	$0.36^{+0.90}_{-0.30}$	973.6/1150

^a Maximum temperature in the pIT models^b $\times 10^{21} \text{ cm}^{-2}$ ^c Defined as L/nr^2 where r is distance from material of density n illuminated by a source of luminosity L **Figure 5.** The best fit GINGA decline from outburst spectrum.

sional excitation becomes important enough to rival radiative recombination, so that the ions are generally in excited rather than ground states. Collisional ionization out of the *excited states*, a process neglected in the assumption of a coronal plasma, can then modify the ionization balance. It also leads to suppression of the dielectronic recombination rate but this is not an important process at the temperatures considered here (e.g. Mewe 1990). For Hydrogen-like ions with atomic number Z in a plasma of temperature T

**Figure 6.** The best fit ASCA anomalous outburst spectrum

(K), deviations from coronal ionization balance are less than a factor 2 when the density $n \leq 4 \times 10^4 Z^2 T^2 \text{ cm}^{-3}$ (e.g. Mewe 1990). Typical temperatures where the hydrogen-like state dominates for oxygen and iron are 10^7 and 10^8 K, respectively, so these elements are out of coronal equilibrium for densities $\geq 2 \times 10^{20}$ and $\geq 2 \times 10^{23} \text{ cm}^{-3}$. The *lower* limit on the density inferred for the boundary layer in the eclipse observations of HT Cas is $\geq 2.5 \times 10^{13} \text{ cm}^{-3}$ (Mukai et al 1996). Thus there is no direct evidence against coronal

equilibrium approximations for the ionization balance in the boundary layer in HT Cas in quiescence. However, the mass accretion rate in SS Cyg in quiescence is nearly two orders of magnitude larger than that in HT Cas, so its boundary layer density may well be substantially higher. The models of Popham and Narayan (1993) suggest a density of $\sim 10^{15} \text{ cm}^{-3}$ for conditions appropriate to the quiescent GINGA spectrum. Again, in outburst the boundary layer density is presumably higher still, but the complexity of the flow makes it difficult to estimate the density of the hard X-ray emitting material. Thus it seems unlikely that the material is as dense as required for coronal ionization balance to become invalid.

A generally more restrictive assumption in the coronal models is that the material is optically thin. In HT Cas the eclipse measure can be used to set constraints on the quiescent emission properties. Assuming that the emission forms a corona of with outer radius $(1 + \delta)R_{WD}$ then the column density through the boundary layer is $N_H \sim 10^{13} \delta^{1/2} R_{WD} \leq 3 \times 10^{21} \text{ cm}^{-2}$ for the maximum value of $\delta = 0.15$. This is optically thin to electron scattering and is also likely to be thin to all the H and He-like Ly α transitions (Matt 1994; Mewe 1990). Even if these lines were optically thick, there is no viable line destruction mechanism for these transitions (see e.g. the discussion in Done et al 1995) so the multiple scatterings have little effect. The plasma is possibly optically thick at iron L (Band et al 1990), but the fact that the iron abundance as measured from the L lines agrees with that derived from the K lines (see section 4.3) argues against this strongly affecting the line emission.

Self photo-ionization of the plasma is potentially important, since there is an intense X-ray flux. The effective ionization parameter for a diffuse source is $\xi = 4\pi cU/n$ where $U \sim \epsilon \delta R_{WD}/c$, and ϵ is the bremsstrahlung emissivity (see e.g. Done et al 1995). Thus $\xi \sim 1.8 \times 10^{-14} n \sim 18$ for a density of $\sim 10^{15}$ and $\delta = 0.15$. This is not high enough to disturb the ionization balance set by the collisional processes, as the ionization states, even for Oxygen for a pure photoionized plasma are much less than those produced in a collisionally ionized plasma at $kT \sim 2 - 10 \text{ keV}$ (Kallman & McCray 1982).

Another process that is neglected in the coronal models is three body recombination (the inverse process of collisional ionization). Here a free electron recombines with the ion, but the recombination energy is given to another free electron rather than being radiated as a free-bound transition. Since this involves two thermal electrons, the rate depends on n_e^2 rather than n_e as for the processes discussed above, so it becomes important only at high densities. Again it efficiently populates the upper excited levels of the ions, so that collisional ionization from excited states can become important and collisional excitation/de-excitation can change the expected line strengths. Cota (1987), quoted by Rees, Netzer and Ferland (1989), states that 3 body processes should be considered for all densities $\geq 10^{10-11} \text{ cm}^{-3}$, which is clearly within the range of densities which are important here. However, it is unclear whether this can have an appreciable effect on the 2–1 line transitions, and Keady et al (1990) show that the coronal approximation for iron ion fractions in a 2 keV plasma holds up to densities $\sim 10^{20} \text{ cm}^{-3}$.

Coronal models also assume that the plasma is in equi-

librium, and so do not apply where the physical conditions vary on timescales which are fast compared to the ionization/recombination timescales e.g. in young supernovae remnants (see e.g. Shull 1982). The collisional ionization timescale, $t_{ion} = (nC)^{-1}$, where C is the collisional ionization rate coefficient, is slowest for H-like iron (Shull and Van Steenberg 1982), where $t_{ion} \sim 10^{16}/(nT^{0.5})$ at $\sim 10^8 \text{ K}$, i.e. 0.1 sec at $n = 10^{13} \text{ cm}^{-3}$. This is much faster than the bremsstrahlung cooling timescale $T_{cool} = 1.5 \times 10^{11} T^{0.5} n^{-1}$ sec for plasma at 10^8 K , and is even rapid compared to the observed X-ray variability (Yoshida et al 1992). This it seems likely that the plasma is hot and dense enough to be in ionization equilibrium.

One density dependent process that will clearly affect the 2–1 line flux is collisional mixing of the 2s and 2p states. For an initially bare nucleus, a recombination cascade can end with an electron transition to the 1s (1^2S) level from either the 2s or 2p state (2^2S or 2^2P). The 2^2S level cannot decay down to ground via a permitted electric dipole transition as it violates the selection rule of $\Delta L = \pm 1$. Its only decay path is a 2 photon electric dipole decay, leading to a continuum rather than an observable line. For recombining initially H-like ions the situation is somewhat more complex, as the cascading electron can have spin either aligned or misaligned with that of the electron in the 1s state. Thus an excited 2s–1s He-like ion can be either 3S , 3P , 1S or 1P , of which the 1S state decays via 2 photons. Thus the $K\alpha$ line from H and He-like ions can be increased by collisional mixing out of the 2^2S and 2^1S level, respectively, and this can strengthen the line by up to 50%, becoming effective for H-like ions of atomic number Z at densities greater than $n \sim 1.8 \times 10^4 Z^{9.3}$ (e.g. Netzer 1996). Thus it should be important for O at densities $\geq 5 \times 10^{12} \text{ cm}^{-3}$, and all elements up to Si and perhaps S for densities of $\sim 10^{15} \text{ cm}^{-3}$. However, it is unlikely to affect iron as this requires densities $\geq 2 \times 10^{17} \text{ cm}^{-3}$. Thus in comparison to the plasma codes calculated with $n = 1 \text{ cm}^{-3}$ we expect the observed Ly α lines from iron in the hot plasma to be representative of the true abundance of iron, while those from the lower Z elements can be enhanced by this process, leading to an overestimate of their abundance by a factor of $\sim 1.2 - 1.5$.

In short, while true coronal equilibrium conditions are not fulfilled in the boundary layer, none of the density, photo-ionization or optical depth effects discussed above are likely to cause the observed sub-solar abundance line intensities from the plasma. The one process that should be important is *enhancement* of the Ly α lines from H and He-like ions of low Z elements by a factor $\sim 1.2 - 1.5$ by collisional mixing transforming states that decay via 2 photons into $K\alpha$ line.

5.2 Abundances

Since coronal models seem to give a good indication of the X-ray line equivalent widths, we can use these to estimate the abundances in SS Cyg. If collisional mixing affects everything other than iron, then all the elements are a factor ~ 3 sub-solar except Si and S, which are probably more like a factor ~ 2 sub-solar. However, this is *not* consistent with the intensity of the observed 6.4 keV fluorescent line from the reflector in the ASCA data, which is weaker in comparison to the reflection continuum than is expected from

material in which all the elements are subsolar by a factor 3. This strongly suggests that the relative abundance of iron with respect to the lighter elements is smaller than the 'solar' definition used here. A recent abundance compilation by Grevasse et al., (1996) gives Fe/H of $\sim 3.2 \times 10^{-5}$ compared to $\sim 4.6 \times 10^{-5}$ in Anders & Grevasse (1989), while most of the lighter elements have abundances within 10% of the Anders & Grevasse (1989) values. Ironically, these newest abundances are very similar to those of Morrison & McCammon (1983) for all the given elements. Without collisional mixing, the plasma in SS Cyg is then uniformly a factor ~ 0.4 below the 'solar' values of Morrison & McCammon (1983) except for Si and S, which are $\sim 0.6 \times$ 'solar'.

5.3 Amount of Reflection

The determination of the amount of reflection is dependent on the assumed abundances. From the above discussion it seems that the abundance ratios in the plasma and reflector are closer to those of Morrison & McCammon (1983). Using these abundances for the reflector as well as the plasma gives the result for SS Cyg that $R = 0.7$ in quiescence, $R = 2.2$ in outburst (see Section 4.4). The amount of reflection in quiescence is *not* consistent with the presence of an optically thick inner disk (see Section 2.2 and 2.3). Either the inner disk is disrupted, or is optically thin. By contrast, the larger amount of reflection in outburst requires that there is additional reflecting material present compared to that in quiescence. This is consistent with a geometry in which the boundary layer extends over the whole white dwarf surface, illuminating both it and an inner disk.

5.4 Ionized Wind

A partially ionized absorber is seen in the ASCA outburst spectrum. The derived ionization state for $\xi \sim 0.2 - 0.5$ (tables 4 and 5) from the `absori` code (see section 4.0) is such that the CIV ionization fraction is at its maximum, with $f_{CIV} \sim 0.1$. This is the upper end of the range found for the blackbody boundary layer or disk illumination models of Hoare and Drew (1993), where f_{CIV} is typically 0.1 – 0.001. The X-ray column density in the warm material in SS Cyg of $N_H \sim 10^{21} \text{ cm}^{-2}$ gives $\dot{M} \sim 2 \times 10^{-12} M_\odot \text{ yr}^{-1}$ using the spherical wind velocity law of Hoare and Drew (1993). Thus $\dot{M} f_{CIV} \sim 2 \times 10^{-13} M_\odot \text{ yr}^{-1}$, much smaller than that inferred from the UV resonance line modelling (e.g. Hoare and Drew 1993), perhaps because the ASCA data are taken towards the end of an outburst (Nousek et al 1993), where the wind may be declining rapidly. We stress that the hard X-ray illumination does have important effects on the ionization structure of the wind, and that the X-ray absorption can give new constraints on the outflowing material which has hitherto only been extensively studied in the UV.

5.5 Continuum Models

The lack of robust theoretical models for the hard X-ray spectrum is a severe problem in interpreting the data. The calculations of Narayan and Popham (1993) are the only

numerical results for the quiescent spectra that can be rigorously tested. However, these are restricted by the 1 dimensional approximations which imply vertical averaging of what is most likely to be a plasma with a stratified temperature structure. In these models the expected spectrum is very like that produced from material that is impulsively heated which then cools via bremsstrahlung alone in a constant pressure/gravitational field. This spectrum is *incompatible* with the GINGA quiescent spectrum, in which the expected cooling gas is not present. Either these models for the quiescent spectrum are wrong, and there is some additional process heating of the gas, or the cooler components are masked by absorption. The ionized wind is unlikely to be important in quiescence, so the only potential absorber is an optically thin inner disk, which could attenuate the emission from the observable part of the hard X-ray boundary layer below the equatorial plane. However, this absorption is *not required* by the data – an equally acceptable description of the spectrum is an X-ray source where the temperature–emissivity relation is weighted towards higher temperatures than expected from simple cooling models.

In outburst there are no detailed models for the temperature–emissivity structure that can currently be compared with the data. However, the integrated luminosity from the hot gas is similar in both outburst and quiescence, although its fractional contribution to the bolometric luminosity is much lower in outburst. The maximum temperature component of the emission is similar in both quiescence and outburst at $\sim 10 - 15 \text{ keV}$ (see section 4.4). As expected, these are always less than the maximum temperature of $\sim 20 \text{ keV}$ produced by a strong shock from material accreting onto a white dwarf mass of $0.8 M_\odot$ and radius of $7 \times 10^8 \text{ cm}$ (Frank et al 1992).

6 CONCLUSIONS

We find a significant reflection signature in all the SS Cyg spectra. This is stronger relative to the illuminating plasma emission in outburst than in quiescence, consistent with models in which the inner disk is optically thick in outburst but optically thin or non-existent in quiescence. The amount of reflection in both quiescence and outburst also supports the idea that the hard X-ray plasma forms a corona over the white dwarf surface, rather than being confined to an equatorial band where the disk/star interaction takes place.

The ASCA outburst spectrum shows significant absorption from partially ionized material, which is probably the outflowing wind inferred from the UV resonance line profiles. The X-ray absorption gives an additional diagnostic window on the wind properties, and suggests rather low mass loss rates of $\sim 10^{-12} M_\odot \text{ yr}^{-1}$. The hard X-ray emission strongly affects the ionization structure of the wind, giving much larger CIV ion fractions than previous blackbody boundary layer photoionisation models.

The ASCA data also give a good determination of the amount of line emission from the plasma, which are a factor ~ 2.5 weaker than expected for solar abundances. We critically examine the assumptions of coronal equilibrium but conclude that the line strengths are representative of the abundances.

The intrinsic plasma emission, when separated from the

effects of reflection and (in outburst) ionized absorption, can then be described by hot plasma with a continuous (power law) temperature–emissivity distribution. In quiescence this distribution is strongly weighted towards the highest temperatures, with very little cooler material present, so that the emission can in practice be modeled by a single temperature plasma. The lack of cool components is in conflict with the predictions of the advective boundary layer models of Narayan & Popham (1993), and with simple models of cooling gas! One possible way to reinstate these models is for the quiescent spectrum to be distorted by partial absorption, such as would be produced if the inner disk is optically thin to electron scattering but optically thick to photoelectric absorption. The flux from the boundary layer below the disk is then absorbed, while that from above the disk is not.

The outburst spectrum by contrast is much softer. It is dominated by the cool components and cannot be modeled as single temperature emission, but the total luminosity of the X-ray emitting gas is very similar to that in quiescence. We review current theoretical models for the hard X-rays in outburst, but none of these address the probable difference in the physical nature of the viscosity between the disk and the boundary layer, or the inherently 3 dimensional nature of the problem. We urge further theoretical modelling, giving the predicted, spatially integrated temperature–emissivity distribution, so that a better understanding of the spectra of dwarf novae can be developed.

7 ACKNOWLEDGEMENTS

We thank Dave Smith for his help with the GINGA data extraction, Bob Popham for discussions about the advective boundary layer models, and John Parker for spatial perception in the reflection calculations. CD acknowledges support from a PPARC Advanced Fellowship. This research has made use of data obtained through the High Energy Astrophysics Science Archive research Center Online Service, provided by the NASA/Goddard Space Flight Center, and from the Leicester Database and Archive Service at the Department of Physics and Astronomy, Leicester University, UK.

REFERENCES

- Armitage P.J., Livio M., Pringle J.E., 1996, *ApJ*, 457, 332
 Arnaud K.A., 1996, In Jacoby G., Barnes J., *Astronomical Data Analysis Software and Systems*, ASP Conf. Series volume 101, p17,
 Anders E., Grevesse N., 1989, *Geochimica et Cosmochimica Acta* 53, 197
 Bailey J., 1981, *MNRAS*, 197, 31.
 Balbus S.A., Hawley J.F., 1991, *ApJ*, 376, 214
 Balbus S.A., Hawley J.F., Stone J.M., 1996, *ApJ*, 467, 76
 Beardmore A P, Done C, Osborne J P & Ishida M 1995, *MNRAS*, 276, 483
 Chen K., Halpern J.P., 1989, *ApJ*, 344, 115
 Cordova F., 1995, In Lewin C.H.G., Van Paradijs J., Van den Heuvel E.P.J., *X-ray Binaries*, CUP, Cambridge, p331
 Cota S.A., 1987, PhD Thesis, Ohio State University.
 Cowley A.P., Crampton D., Hutchings J.B., 1980, *ApJ*, 241, 269
 Cropper M., Ramsey G., Wu K., 1996, *MNRAS*, submitted
 Done C., Mulchaey J.S., Mushotzky R.F., Arnaud K.A., 1992, *ApJ*, 395, 275
 Done C., Osborne J.P., Beardmore A.P., 1995, *MNRAS*, 276, 483
 Drew J.E., 1993, In Regev O., Shaviv J., eds, *Proc 2nd Technion Haifa Conf.*, Ann. Israel Phys. Soc., p128
 Frank J., King A.R., Raine D., 1992, in *Accretion Power in Astrophysics*, 2nd edn. CUP, Cambridge
 George I. Fabian A.C., 1991, *MNRAS*, 249, 352
 Grevasse N., Noels A., Sauval A.J., 1996, In Holt S.S., Sonneborn G., eds, *Cosmic Abundances*, ASP conference series 99, p117.
 Hayashida K., et al., 1989, *PASJ*, 41, 373
 Hoare M.G., Drew J.E., 1991, *MNRAS*, 249, 452
 Hoare M.G., Drew J.E., 1993, *MNRAS*, 260, 647
 Hujerirat A., 1995, *A&A*, 295, 268
 Johnson R.M., Fabian A.C., Edge A.C., Thomas P.A., 1992, *MNRAS*, 255, 431
 Kallman T.R., McCray R., 1982, *ApJ. Supp.*, 50, 263
 Keady J.J., Huebner W.F., Abdallah J., Magee N.H., 1990, In Brinkmann W., ed., *Physical Processes in Hot Cosmic Plasmas*, Kulwer Acad. Publ., Dordrecht, p181
 King A.R., Shaviv G., 1985, *Nature*, 308, 519
 Kley W., 1989, *A&A*, 222, 141
 Kluzniak W., 1987, PhD Thesis, Stanford University.
 Lemen J.R., Mewe R., Schrijver C.J., Fludra A., 1989, *ApJ*, 341, 474
 Lightman A.P., White T.R., 1988, *ApJ*, 335, 57
 Livio M., Pringle J.E., 1992, *MNRAS*, 259, 23p
 Magdziarz P., Zdziarski A.A., 1995, *MNRAS*, 273, 837
 Matt G., 1994, *MNRAS*, 267, L17
 Matt G., Perola G.C., Piro L., 1991, *A&A*, 247, 25
 Mauche C.W., Raymond J.C., 1987, *ApJ*, 323, 690
 Mauche C.W., Raymond J.C., Cordova F.A., 1988, *ApJ*, 335, 829
 Mauche C.W., Raymond J.C., Mattei J.A., 1995, *ApJ*, 446, 842
 Mewe R., 1990, In Brinkmann W., ed., *Physical Processes in Hot Cosmic Plasmas*, Kulwer Acad. Publ., Dordrecht, p39
 Meyer F., Meyer–Hofmeister E., 1994, *A&A*, 288, 175
 Morrison R., McCammon D., 1983, *ApJ*, 270, 119
 Mukai K., Wood J.H., Naylor T., Schlegel E.M., Swank J.H., 1996, *ApJ*, in press
 Narayan R., Popham R., 1993, *Nature*, 362, 820
 Nauenberg M., 1972, *ApJ*, 175, 417
 Netzer H., 1996, *ApJ*, in press
 Nousek J.A., Baluta C.J., Corbet R.H.D., Mukai K., Osborne J.P., Ishida M., 1994, *ApJ*, 436, L19
 Osaki Y., 1996, *PASP*, 108, 39
 Patterson J., Raymond J.C., 1985a, *ApJ*, 292, 535
 Patterson J., Raymond J.C., 1985b, *ApJ*, 292, 550
 Ponman T.R., Belloni T., Duck S.R., Verbunt F., Watson M.G., Wheatley P.J., Pfeffermann E., 1995, *MNRAS*, 276, 495
 Popham R., Narayan R., 1995, *ApJ*, 442, 337
 Press W.H., Teukolsky S.A., Vetterling W.T., Flannery B.P., 1993, *Numerical Recipes*, 2nd edn, CUP, Cambridge
 Pringle J.E., 1977, *MNRAS*, 178, 195
 Pringle J.E., Savonije G.J., 1979, *MNRAS*, 187, 777
 Rees M.J., Netzer H., Ferland G.J., 1989, *ApJ*, 347, 640
 Reynolds C.S., Fabian A.C., Inoue H., 1995, *MNRAS*, 276, 1311
 Shull J.M., 1982, *ApJ*, 262, 308
 Shull J.M., Van Steenberg M., 1982, *ApJ. Supp.*, 48, 95
 Tout C.A., Pringle J.E., 1992, 259, 604
 Turner M.J.L., et al., 1989, *PASJ*, 41, 345
 Tylenda R., 1981, *Acta Astr.*, 31, 127
 van Teeseling A., Beuermann K., Verbunt F., 1996, *A&A*, 315, 467
 van Teeseling A., Kaastra J.S., Heise J., 1996, *A&A*, 312, 186
 Verbunt F., et al., 1984, *MNRAS*, 210, 197
 Warner B., 1995, In *Cataclysmic Variable Stars*, CUP, Cambridge
 Williams O.R., et al., 1992, *ApJ*, 389, 157
 Yoshida K., Inoue H., Osaki Y., 1992, *PASJ*, 44, 537

Zycki P.T., Krolik J.H., Zdziarski A.A., Kallman T.R., 1994, *ApJ.*, 437, 597

8 APPENDIX

The angle η between the X-ray emitting source and the line of sight is then given by

$$\cos \eta = \sin i \sin \theta \sin \phi + \cos i \cos \theta$$

The reflection spectrum from each small segment of the white dwarf underlying the boundary layer can be approximated by an isotropically illuminated slab viewed at inclination η . Thus the average inclination between the reflector and the observer is given by averaging η over all angles at which the boundary layer emission can be seen. If the disk is optically thick and extends down to the white dwarf surface (figure 2a) then this is given by

$$\begin{aligned} \overline{\eta(i, \beta)} &= \frac{2}{N} \int_0^{\pi/2} d\phi \int_{\pi/2-\beta}^{\pi/2} d\theta \eta(\theta, \phi, i) \sin \theta \\ &+ \frac{2}{N} \int_{-\phi_{\min}}^0 d\phi \int_{\pi/2-\beta}^{\theta_{\max}} d\theta \eta(\theta, \phi, i) \sin \theta \end{aligned} \quad (1)$$

where the normalisation N is given by equation (1) but with all the $\eta(\theta, \phi, i)$ terms removed from the integrand, and

$$\begin{aligned} \phi_{\min} &= \pi/2 \dots \beta \geq i \\ &= \arcsin \left[\frac{\tan \beta}{\tan i} \right] \dots \beta \leq i \\ \theta_{\max} &= \arctan \left(\frac{-1}{\sin \phi \tan i} \right) \end{aligned}$$

This needs to be integrated numerically. The inclination angle of SS Cyg is thought to be $i = 37^\circ$ (Cowley et al 1980). For the two limiting values of $\beta \rightarrow 0^\circ$ and $\beta \rightarrow 90^\circ$ the angle of the emission to the line of sight is 67° and 53° , respectively.

Alternatively, if the inner disk does not obscure the boundary layer (figure 2b) then the mean inclination angle is

$$\begin{aligned} \overline{\eta(i, \beta)} &= \frac{2}{N} \int_{\phi_{\min}}^{\pi/2} d\phi \int_{\pi/2-\beta}^{\pi/2+\beta} d\theta \eta(\theta, \phi, i) \sin \theta \\ &+ \frac{2}{N} \int_0^{\phi_{\min}} d\phi \int_{\pi/2-\beta}^{\pi+\theta_{\max}} d\theta \eta(\theta, \phi, i) \sin \theta \\ &+ \frac{2}{N} \int_{-\phi_{\min}}^0 d\phi \int_{\pi/2-\beta}^{\theta_{\max}} d\theta \eta(\theta, \phi, i) \sin \theta \end{aligned} \quad (2)$$

where θ_{\max} and ϕ_{\min} are given as before, and the normalisation N is given by equation (2) with all the $\eta(\theta, \phi, i)$ terms removed from the integrand.

Again, the limiting case for $\beta \rightarrow 0$ is a mean inclination of 53° (the presence or absence of a disk makes no difference if the boundary layer is limited to the equatorial plane), while that for $\beta \rightarrow 90^\circ$ is 57° .

Given that all these limits are very close to each other, the mean angle at which we see the boundary layer in SS Cyg is approximately 60° , irrespective of whether or not there is

an inner disk or the extent of the boundary layer. Thus the reflection component from the white dwarf surface in SS Cyg is approximately that expected from an isotropically illuminated slab viewed at 60° .